Available online at www.sciencedirect.com
ScienceDirect
Applied Mathematics and Computation 196 (2008) 448–457
APPLIED MATHEMATICS AND COMPUTATION
www.elsevier.com/locate/amc

Numerical study for a model of tumor virotherapy

Jin Wang [a,*], Jianjun Tian [b]

[a] Department of Mathematics, Box 90320, Duke University, Durham, NC 27708, USA
[b] Mathematical Biosciences Institute, The Ohio State University, Columbus, OH 43210, USA

Abstract

In this paper, we present a computational mathematical model to investigate the efficacy of tumor virotherapy using oncolytic viruses. A numerical algorithm, which is stable and second-order accurate, is developed to compute the growth of the tumor. Results from the numerical simulation have matched the experimental measurements, and validated the significance of the oncolytic viral therapy. Moreover, our numerical results suggest that this therapy can be further improved by increasing the burst size of viruses and using cyclophosphamide (CPA) treatments.

Keywords: Computational biology; Tumor growth; Oncolytic virotherapy

1. Introduction

Oncolytic viruses have been providing a promising way for tumor treatment. Such viruses infect tumor cells and replicate inside them, without harming healthy normal cells, and eventually cause lysis. The newly formed viruses during lysis then spread throughout the tumor and infect other tumor cells. Although much progress has been made in both the theoretical study and clinical trials of oncolytic viruses [6,8,12,22,23], this therapy, unfortunately, has not yet met its expectations. One main reason for the degeneration of its efficacy is due to the innate immune response. It has been manifested that the immune system can destroy both the viruses and infected tumor cells [4].

Fulci et al. [10] recently reported experimental results of the oncolytic viral therapy on brain tumors in rats. It was found that although the viruses can significantly extend the rats' lives (up to 50%), the innate immune system inhibits the oncolysis and enables the tumors to grow, eventually killing the rats. Based on the experimental results, Friedman et al. [9] proposed a mathematical model to study the efficacy of tumor virotherapy, taking into account the immune response. The formulation consists of a non-linear PDE system in a spherical domain with a moving boundary, together with suitable boundary and initial conditions. This model appears to be a good representation of the complicated biomedical process, and allows a comprehensive study of the interaction between the tumor cells, oncolytic viruses and immune system. Since the problems is strongly

* Corresponding author.
E-mail addresses: wang@math.duke.edu (J. Wang), tianjj@mbi.ohio-state.edu (J. Tian).

0096-3003/$ - see front matter
doi:10.1016/j.amc.2007.06.016

non-linear, it is impossible to find analytic solutions. Hence, numerical simulation offers an excellent way to analyze the model and improve our understanding of the fundamental mechanism involved.

In this paper, we numerically study the tumor virotherapy model originally developed in [9]. After a brief introduction of the mathematical formulation, the numerical algorithm is presented, with sufficient details given separately in Appendix. Then, results from the numerical simulation are described and two possible approaches to improve the oncolytic virotherapy are discussed. Finally, a summary is made for the main results of this study and some possible generalizations are mentioned.

2. Mathematical formulation

The equations presented in the current paper are slightly different from those in [9] in that we use a partially non-dimensionalized form. We consider a spherical tumor. Let X, Y, Z and N be the volume fractions of uninfected tumor cells, infected tumor cells, immune cells and dead tumor cells, respectively. Since the total cell density is normally a constant, we have

$$X + Y + Z + N = 1. \tag{1}$$

Eq. (1) enables us to drop one variable, N. In addition, we denote V the density of free virus particles, U the cell velocity and R the moving boundary of the tumor.

We assume spherical symmetry in this study, and let ρ be the radial distance from the tumor center. The motion of all the cells is governed by a convection field in the radial direction. The virus particles, in contrast, undergo a diffusion process since a virus particle (with a typical diameter of 1.3×10^{-4} mm) is much smaller than a cell (with a typical diameter of 1.0×10^{-2} mm). As a result, we obtain

$$\frac{\partial X}{\partial t} + \frac{1}{\rho^2}\frac{\partial}{\partial \rho}(\rho^2 UX) = \lambda X - \beta XV, \tag{2}$$

$$\frac{\partial Y}{\partial t} + \frac{1}{\rho^2}\frac{\partial}{\partial \rho}(\rho^2 UY) = \beta XV - kZY - \delta Y, \tag{3}$$

$$\frac{\partial Z}{\partial t} + \frac{1}{\rho^2}\frac{\partial}{\partial \rho}(\rho^2 UZ) = sYZ - wZ^2, \tag{4}$$

$$\frac{\partial V}{\partial t} - D\frac{1}{\rho^2}\frac{\partial}{\partial \rho}\left(\rho^2 \frac{\partial V}{\partial \rho}\right) = \delta Y - k_0 VZ - \gamma V, \tag{5}$$

$$\frac{1}{\rho^2}\frac{\partial}{\partial \rho}(\rho^2 U) = \lambda X - \mu(1 - X - Y - Z) + sYZ - wZ^2, \tag{6}$$

where $0 \leqslant \rho \leqslant R(t)$, $t > 0$ and where t is the temporal variable. In this model, ρ and t are dimensional quantities and their units are millimeter and hour, respectively. The parameter values of $\lambda, \beta, k, \delta, s, w, D, k_0, \gamma$ and μ are given in Table 1. Among these parameters, $\lambda, \delta, w, D, \mu$ have been reliably determined, based on experimental data [10] and commonly accepted values [3,7,13,15,17]. The parameters k, s, k_0, γ were first estimated rather crudely from the experiments [10], then were determined, through trial and error, in matching the numerical results with the experimental ones for the volume fractions of the cells and the growth rate of the tumor. Finally, the parameter β is proportional to the burst size of viruses, b. Indeed $\beta = 0.07b$, where $b = 50$ for the virus hrR3 used by Fulci et al. [10]. The value of b measures the number of new viruses per one infected cell, and is highly virus-dependent. We will explore the effects of different burst sizes in our numerical study.

The moving boundary $R(t)$ satisfies the kinematic condition

$$\frac{\mathrm{d}R(t)}{\mathrm{d}t} = U(R(t), t). \tag{7}$$

Table 1
The values of the parameters in Eqs. (2)–(6)

Parameter	λ	β	k	s	w	D	δ	k_0	γ	μ
value	2.0	3.5	2.0	56	20	3.6	5.6	1.0	2.5	2.1

At the tumor center, the spherical symmetry requires

$$U(0,t)=0 \quad \text{and} \quad \frac{\partial V}{\partial \rho}(0,t)=0. \tag{8}$$

Meanwhile, we require the virus particles do not cross the boundary [8,14,20]. Hence,

$$\frac{\partial V}{\partial \rho}(R(t),t)=0. \tag{9}$$

3. Numerical algorithm

The presence of a moving boundary $R(t)$ makes direct design of numerical methods difficult. To overcome this difficulty, we map the moving boundary into a fixed one by introducing a new coordinate,

$$r=\frac{\rho}{R(t)}. \tag{10}$$

Consequently, the original Eqs. (2)–(6) are transformed to

$$\frac{\partial X}{\partial t}+\frac{U-rR'}{R}\frac{\partial X}{\partial r}=F_1, \tag{11}$$

$$\frac{\partial Y}{\partial t}+\frac{U-rR'}{R}\frac{\partial Y}{\partial r}=F_2, \tag{12}$$

$$\frac{\partial Z}{\partial t}+\frac{U-rR'}{R}\frac{\partial Z}{\partial r}=F_3, \tag{13}$$

$$\frac{\partial V}{\partial t}-\left(\frac{rR'}{R}+\frac{2D}{R^2 r}\right)\frac{\partial V}{\partial r}-\frac{D}{R^2}\frac{\partial^2 V}{\partial r^2}=F_4, \tag{14}$$

$$\frac{1}{Rr^2}\frac{\partial}{\partial r}(r^2U)=F_5, \tag{15}$$

where $0\leqslant r\leqslant 1$, $t>0$, and where $R'=\frac{dR}{dt}$. The expressions on the right-hand sides are given by

$$\begin{aligned}
F_1&=\lambda X-\beta VX-FX,\\
F_2&=\beta VX-kYZ-\delta Y-FY,\\
F_3&=sYZ-wZ^2-FZ,\\
F_4&=\delta Y-k_0VZ-\gamma V,\\
F_5&=F,
\end{aligned}$$

where

$$F=\lambda X-\mu(1-X-Y-Z)+sYZ-wZ^2.$$

The boundary conditions (7)–(9) become

$$\frac{dR(t)}{dt}=U(1,t), \tag{16}$$

$$U(0,t)=0, \tag{17}$$

$$\frac{\partial V}{\partial r}(0,t)=0 \quad \text{and} \quad \frac{\partial V}{\partial r}(1,t)=0. \tag{18}$$

In order to start the numerical simulation, we also need to specify the initial values of these variables. They are given in such a way as to match the experimental conditions [10]. In particular, a Gaussian distribution is used to represent the initial profile of the viruses, which were injected into the center of the tumor in the experiment.

$$R(0) = 2 \text{ mm}, \tag{19}$$

$$V(r,0) = a\mathrm{e}^{-\frac{4r^2}{a^2}}, \quad \text{where} \quad a\int_0^1 r^2\mathrm{e}^{-\frac{4r^2}{a^2}}\,\mathrm{d}r = 0.45, \tag{20}$$

$$X(r,0) = 0.84, \quad Y(r,0) = 0.10, \quad Z(r,0) = 0.06. \tag{21}$$

Based on the mapped equations, we construct our numerical methods as follows. The Adams–Bashforth method [1] is applied to advance the tumor radius R in time. At each time step, the Leapfrog scheme [19] is employed to solve the hyperbolic Eqs. (11)–(13) for X, Y and Z. Then, we calculate U by applying the Trapezoidal Rule [2] in the numerical integration for (15). Finally, we use the fully implicit backward difference formula [16] to update V. The details of the numerical algorithm are presented in the Appendix. We have found that the numerical algorithm achieves second-order accuracy in both time (t) and space (r).

4. Numerical results

The numerical methods (described in the Appendix) have been applied to simulate the tumor model. Fig. 1 shows the impact of oncolytic viruses on the evolution of the tumor radius, R. The dashed line represents the case without virus and is based on the experimental data [10]. In particular, $R = 2$ mm at $t = 0$, $R = 4$ mm at $t = 72$ h and $R = 6$ mm at $t = 144$ h. The rats were dead when $R = 6$ mm as the tumors were big enough to kill them. The solid line shows the numerical result in the case with the virus hrR3 whose burst size is $b = 50$. We observe that for the first few hours, the radius increases as fast as in the case without virus. The reason is that initially the viruses are concentrated in the center of the tumor and do not have much impact on the tumor growth. However, as the viruses spread out in the tumor, the growth rate of the tumor is significantly slowed down, as is clearly shown in the figure. As a result, R reaches 6 mm at $t \approx 220$ h. The numerical result indeed matches the experimental measurement. It is reported in [10] that the rats can live up to 9 days (216 h) with the virus hrR3. The significance of the therapy is clear: the lives of rats can be extended up to 50% by using a certain type of virus.

A main purpose of this study is to explore possible improvements of the oncolytic therapy. To this end, we consider the following two approaches:

(1) increasing the burst size b, which can promote the infection;
(2) adding CPA drugs, which can suppress the immune system.

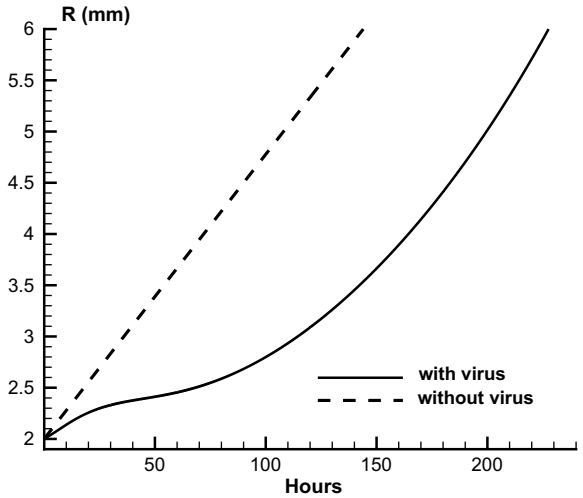

Fig. 1. Evolution of tumor radius R in the cases without virus and with the virus hrR3 ($b = 50$).

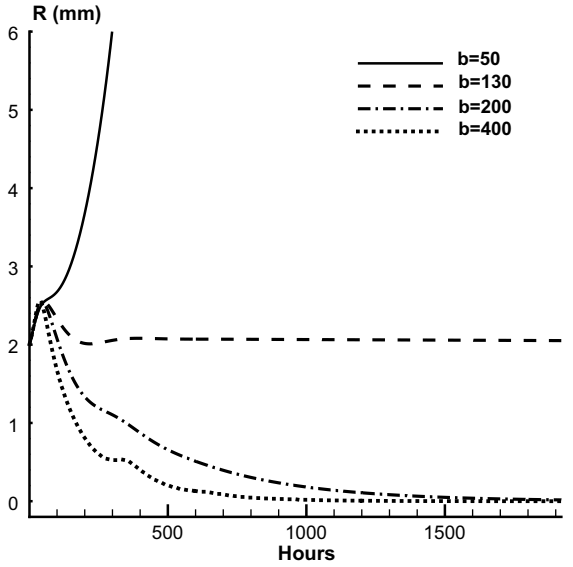

Fig. 2. Evolution of tumor radius R with different burst sizes.

Let us investigate the effects of burst sizes first. The virus hrR3 has a relatively small burst size, $b = 50$. By selecting some other types of viruses, it is possible to make b much bigger. The bigger b, the faster the viruses replicate, and the stronger the infection is. Fig. 2 shows the evolution of R with different choices of burst sizes. Here, we consider a much longer period which is 80 days, or 1920 h, to check the long-term effects of the therapy. For $b = 50$, R increases to 6 mm in about 9 days. This is the case we already discussed. For any value between 50 and 130, R increases as well, but with slower rate than that for $b = 50$. For $b = 130$, R first increases slightly, then decreases to 2 mm, and keep this value forever. For $b > 130$, say, $b = 200$ or 400, R shrinks to an extremely small size over time. The results indicate that $b = 130$ is a critical value for the burst size. When $b < 130$, the tumor grows; when $b > 130$, the tumor decays.

However, a closer examination of the results reveals that the uninfected tumor cells do not decrease to 0 even though the tumor size can be kept very small. For convenience of illustration, we take the spatial average of $X(\rho, t)$ over the whole sphere to obtain a function, X_{avg}, which is only dependent on time:

$$X_{\text{avg}}(t) = \frac{3}{R^3(t)} \int_0^{R(t)} X(\rho, t)\rho^2 \, \mathrm{d}\rho. \tag{22}$$

We then plot X_{avg} vs. t in Fig. 3 with different choices of burst sizes. It is clearly shown that as t is getting bigger, X_{avg} approaches $1.00, 0.35, 0.20$ and 0.10, for $b = 50, 130, 200$ and 400, respectively. (Note that when b is large, say 400, there is a strong competition between tumor cells, viruses and immune cells, especially in the initial stage. This results in an oscillatory behavior of X_{avg}. Over time, however, the oscillation relaxes to its mean value, about 0.10 for $b = 400$). Hence, the uninfected tumor cells persist even with large values of burst sizes, and there is a good chance that these tumor cells can migrate into other areas in the brain and develop a secondary tumor. It is, therefore, necessary to use some CPA treatment to reduce such a risk.

The CPA drugs, formally called cyclophosphamide [21], can effectively suppress the innate immune response and thereby enhance oncolysis. Mathematically, this effect is represented by adding a negative term to Eq. (4) for Z, the immune cells,

$$\frac{\partial Z}{\partial t} + \frac{1}{\rho^2}\frac{\partial}{\partial \rho}(\rho^2 ZU) = sYZ - wZ^2 - P(t)Z,$$

where $P(t)$ represents the CPA treatment and is a predetermined function of t. Here we consider three protocols of CPAs: traditional CPA, weekly CPA and constant CPA, as illustrated in Fig. 4.

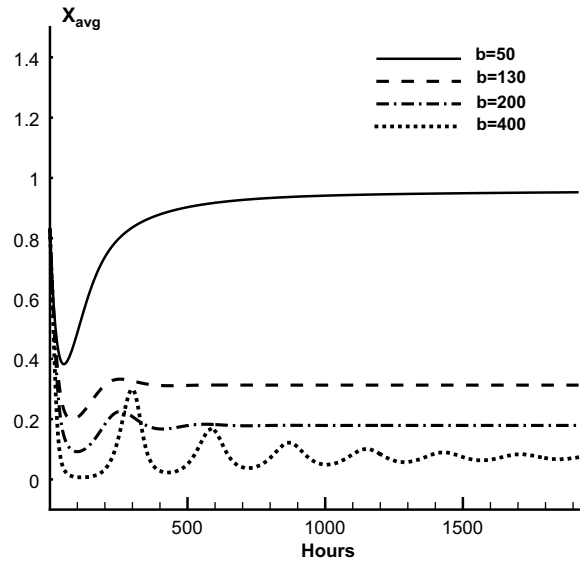

Fig. 3. Evolution of X_{avg} with different burst sizes.

We apply these three types of CPA treatments in the tumor model and compare their performance. Fig. 5 shows the results for X_{avg} vs. t with $b = 130$. There is almost no improvement with the traditional CPA treatment. However, the other two types of CPA treatments do make a difference. The constant CPA reduces X_{avg} from 0.35 to approximately 0.25. This is also true for the weekly CPA, provided that we take the average in

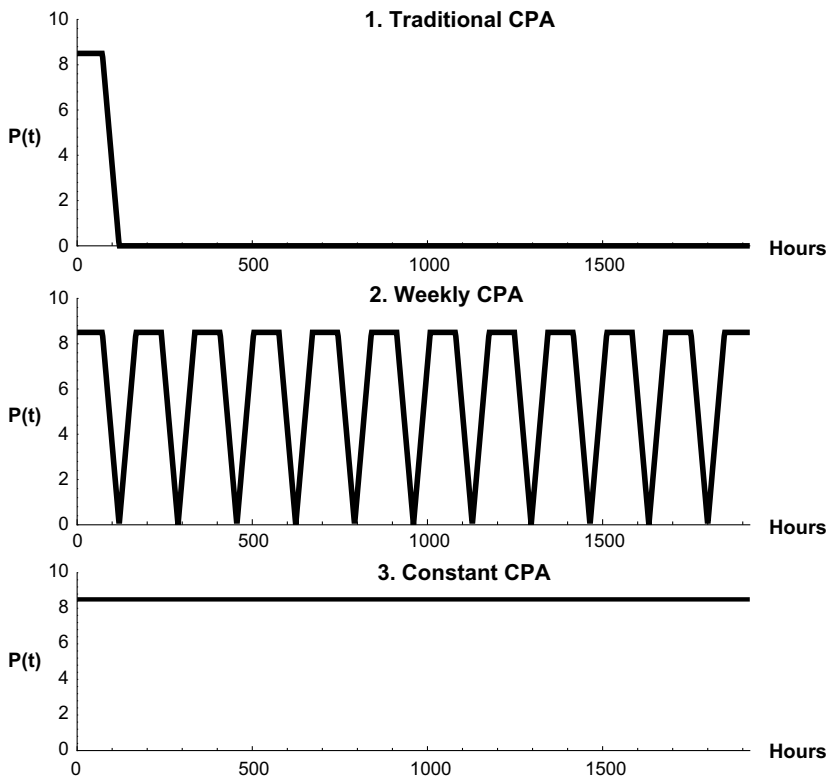

Fig. 4. Three types of CPA, with maximum value 8.5 in each case.

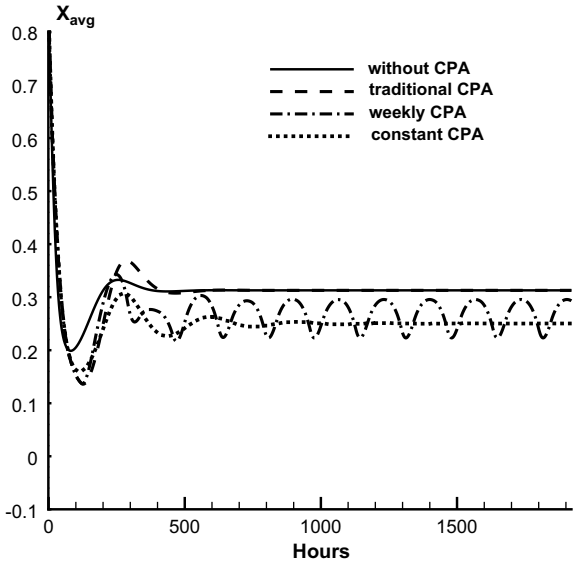

Fig. 5. Evolution of X_{avg} with different CPAs for the burst size $b = 130$.

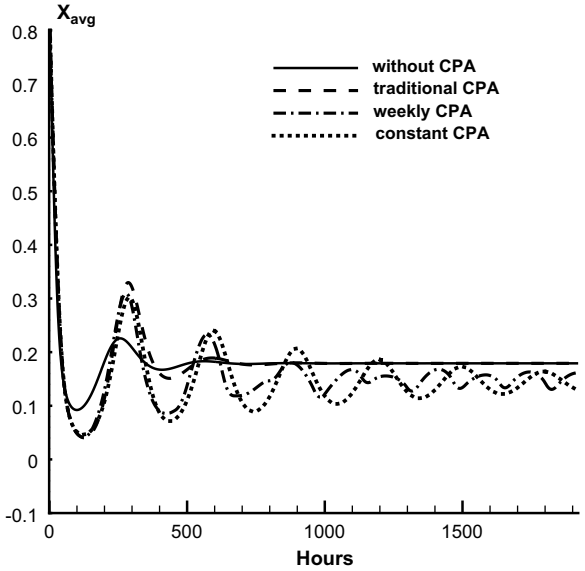

Fig. 6. Evolution of X_{avg} with different CPAs for the burst size $b = 200$.

time of the oscillations. Fig. 6 shows the results with $b = 200$ and we observe similar pattern. In particular, the weekly CPA and constant CPA treatments reduce X_{avg} from 0.20 to approximately 0.12, in average, over the time. Although it is not possible to eliminate all the tumor cells, the risk of secondary tumors is reduced by using such CPA treatments.

5. Discussion

We have developed a numerical algorithm, which ensures uniform second-order accuracy in both space and time, to simulate a mathematical model of tumor virotherapy, i.e., Eqs. (2)–(6) subject to boundary conditions

(7)–(9). The numerical results agree with the experimental measurements. In particular, it is shown that the oncolytic viruses can significantly slow down the growth of tumors.

We have explored two approaches to improve the efficacy of the virotherapy: by increasing the burst size b and by adding CPA treatment. We have found that the tumors decay when $b > 130$. However, even though the tumor size can be kept very small by using viruses of large burst sizes, there are still certain amount of uninfected tumor cells which give rise to the risk of secondary tumors. Using weekly CPA or constant CPA treatments can reduce these tumor cells and further improve the therapy.

Our model is concerned with a spherical geometry, which is a reasonable approximation for most tumors. In some situations, however, it might be worthwhile to study the virotherapy on tumors of arbitrary shape. By using the mass conservation and convection/diffusion processes for the cells/viruses, the governing equations can be naturally generalized from one spatial dimension to three-dimension (3D), although large-scale computations can be expected for the 3D problem.

In addition to higher spatial dimensions, the current computational model can be extended in a few other interesting directions. One example is to take into account the side effects of CPA treatments so that our model can predict the practical efficacy of the virotherapy more accurately. Another example is to simulate the formation and growth of multiple tumors, and study the combined efficacy of possible treatments.

Acknowledgements

This work is partially supported by the National Science Foundation upon agreement No.0112050. The authors thank Prof. Greg Baker for many helpful discussions during the preparation of this paper.

Appendix A

The numerical simulation of Eqs. (11)–(15) is essentially a time-marching problem. Let us denote the numerical solution at the nth time step by

$$(R^n, X^n, Y^n, Z^n, U^n, V^n).$$

Suppose we know the numerical solution at the time steps $n-1$ and n, and we want to advance the solution to the next time step $n+1$. The details are described below.

First, application of the Adams–Bashforth method to (16) yields

$$R^{n+1} = R^n + \frac{\Delta t}{2}(3U^n - U^{n-1}). \tag{23}$$

To start (23), R^0 is provided by the initial condition (19) and R^1 is calculated by the Trapezoidal Rule.

Next, we solve the hyperbolic Eqs. (11)–(13). For illustration, we consider the numerical discretization of (11). Let

$$A = \frac{U - rR'}{R}.$$

Application of the leapfrog scheme to (11) yields

$$\frac{X_j^{n+1} - X_j^{n-1}}{2\Delta t} + A_j^n \frac{X_{j+1}^n - X_{j-1}^n}{2\Delta r} = (F_1)_j^n, \tag{24}$$

where the subscript j refers to the jth grid point in the radial direction and $j = 1,2,\cdots,J-1$, with $J\Delta r = 1$. The Crank–Nicolson method [19] is used for start-up. Noting (16) and (17), it is clear to see

$$A = 0, \quad \text{when} \quad r = 0 \quad \text{or} \quad 1.$$

Therefore, at the two ends $r = 0,1$, (11) is reduced to an ODE

$$\frac{dX}{dt} = F_1. \tag{25}$$

Central differences, which are consistent with the leapfrog scheme, are used to solve (25).

One common problem associated with the leapfrog method is that when applied to non-linear equations, the method often becomes unstable due to the fact that odd and even mesh points are completely decoupled [18]. Fortunately, this mesh drifting instability can be cured by coupling the two meshes through a simple average in time

$$X_j^n = \frac{1}{2}(X_j^{n+1} + X_j^{n-1}), \tag{26}$$

which still keeps the second-order accuracy of the leapfrog method. We have found that stability can be recovered, subject to the usual CFL condition [5], by merely implementing (26) in every 10 or 20 time steps. Y and Z are updated in a similar way.

Once $X^{n+1}, Y^{N+1}, Z^{n+1}$ are known, we calculate U^{n+1} by applying the Trapezoidal rule to (15),

$$r_{j+1}^2 U_{j+1}^{n+1} - r_j^2 U_j^{n+1} = \frac{R^{n+1}}{2}\Delta r[r_{j+1}^2 (F_5)_{j+1}^{n+1} + r_j^2 (F_5)_j^{n+1}]. \tag{27}$$

Note that F_5 is independent of U and V, so that Eq. (27) explicitly identifies the recurrence relation between U_{j+1}^{n+1} and U_j^{n+1}, with U_0^{n+1} determined by the boundary condition (17).

Finally, we solve the parabolic Eq. (14). It is rewritten, for convenience of discussion, by

$$\frac{\partial V}{\partial t} + A_1 \frac{\partial V}{\partial r} + A_2 \frac{\partial^2 V}{\partial r^2} = F_4, \tag{28}$$

where

$$A_1 = -\left(\frac{rR'}{R} + \frac{2D}{R^2 r}\right), \quad A_2 = -\frac{D}{R^2}.$$

Note that A_1 and A_2 are independent of V. Meanwhile, R^{n+1}, X^{n+1}, Y^{n+1}, Z^{n+1} and U^{n+1} are already known so that F_4 becomes a linear function of V^{n+1}. Therefore, (28) is indeed a linear parabolic equation at the time step $n+1$. An implicit method is normally a better choice for such an equation than an explicit one, since the latter would impose stringent constraint on the time step size to ensure stability. Here, we use the second-order implicit BDF method in time and central differences in space to approximate (28),

$$\frac{3V_j^{n+1} - 4V_j^n + V_j^{n-1}}{2\Delta t} + (A_1)_j^{n+1}\frac{V_{j+1}^{n+1} - V_{j-1}^{n+1}}{2\Delta r} + (A_2)_j^{n+1}\frac{V_{j+1}^{n+1} - 2V_j^{n+1} + V_{j-1}^{n+1}}{\Delta r^2} = (F_4)_j^{n+1}. \tag{29}$$

The discretized Eq. (29) yields a linear, tridiagonal algebraic system

$$b_j V_{j-1}^{n+1} + d_j V_j^{n+1} + a_j V_{j+1}^{n+1} = S_j, \quad j = 1, 2, \cdots, J, \tag{30}$$

where

$$b_j = \frac{2\Delta t}{\Delta r^2}(A_2)_j^{n+1} - \frac{\Delta t}{\Delta r}(A_1)_j^{n+1},$$
$$d_j = 3 - \frac{4\Delta t}{\Delta r^2}(A_2)_j^{n+1} + 2k_0 \Delta t Z_j^{n+1} + 2\gamma\Delta t,$$
$$a_j = \frac{2\Delta t}{\Delta r^2}(A_2)_j^{n+1} + \frac{\Delta t}{\Delta r}(A_1)_j^{n+1},$$

and where

$$S_j = 4V_j^n - V_j^{n-1} + 2\delta\Delta t Y_j^{n+1}.$$

Such an algebraic system can be solved very rapidly [11]. Once V^{n+1} is calculated, the advancement of solution to the time step $n+1$ is complete. We then start the next cycle of marching in time.

References

[1] D.A. Anderson, J.C. Tannehill, R.H. Pletcher, Computational Fluid Mechanics and Heat Transfer, Hemisphere Publishing Corporation, 1984.
[2] U. Ascher, R. Matteij, R. Russell, Numerical Solution of Boundary Value Problems for Ordinary Differential Equations, Prentice Hall, New Jersey, 1988.
[3] M. Chaplain, V. Kuznetsov, Z. James, A. Stepanova, Spatio-temporal dynamics of the immune system response to cancer, Mathematical Models in Medical and Health Sciences, Vanderbilt University Press, 1998.
[4] E.A. Chiocca, Oncolytic viruses, Nat. Rev. Cancer 2 (2002) 938–950.
[5] R. Courant, K.O. Friedrichs, H. Lewy, Uber die partiellen differenzengleichungen der Mathematischen Physik, Mathematishe Annalen 100 (1928) 32–74.
[6] L.K. Csatary et al., MTH-68/H oncolytic viral treatment in human high-grade gliomas, J. Neurooncol. 67 (2004) 83–93.
[7] J.F. Fowler, The phantom of tumor treatment – continually rapid proliferation unmasked, Radiother. Oncol. 22 (1991) 156–158.
[8] A. Friedman, Y. Tao, Analysis of a model of a virus that replicates selectively in tumor cells, J. Math. Biol. 47 (2003) 391–423.
[9] A. Friedman, J.P. Tian, G. Fulci, E.A. Chiocca, J. Wang, Glioma virotherapy: the effects of innate immune suppression and increased viral replication capacity, Cancer Res. 66 (2006) 2314–2319.
[10] G. Fulci et al., Cyclophosphamide enhances glioma virotherapy by inhibiting innate immune responses, Proc. Natl. Acad. Sci. 103 (2006) 12873–12878.
[11] G.H. Golub, C.F. Van Loan, Matrix Computations, The Johns Hopkins University Press, 1996.
[12] R.M. Lorence et al., Overview of phase I studies of intravenous administration of PV701, an oncolytic virus, Curr, Opin. Mol. Ther. 5 (2003) 618–624.
[13] V. Kusnetzov, V. Zhivoglyadov, L. Stepanova, Kinetic approach and estimation of the,parameters of cellular interaction between the immune system and a tumor, Arch. Immunol. Therap. Exper 41 (1993) 21–32.
[14] K. Oelschlager, The spread of a parasitic infection in a spatially distributed host, J. Math. Biol. 30 (1992) 321–354.
[15] S.S. Olmsted, J.L. Padgett, A.I. Yudin, K.J. Whaley, T.R. Moench, R.A. Cone, Diffusion of macromolecules and virus-like particles in human cervical mucus, Biophys. J. 81 (2001) 1930–1937.
[16] M.N. Ozisik, Finite Difference Methods in Heat Transfer, CRC Press, 1994.
[17] A.L. Pecora et al., Phase I trial of intraveneous administration of PV701, an oncolytic virus, in patients with advanced solid cancers, J. Clin. Oncol. 20 (2002) 2251–2266.
[18] W.H. Press, B.P. Flannery, S.A. Teukolsky, W.T. Vetterling, Numerical Recipes in Fortran: The Art of Scientific Computing, Cambridge University Press, 1992.
[19] R.D. Richtmyer, K.W. Morton, Difference method for initial value problems, John Wiley and Sons, 1967.
[20] Y. Tao, Q. Guo, The competitive dynamics between tumor cells, a replication-competent virus and immune response, J. Math. Biol. 51 (2005) 37–74.
[21] H. Wakimoto, G. Fulci, E. Tyminski, E.A. Chiocca, Altered expression of antiviral cytokines mRNAs associated with cyclophosphamide's enhancement of viral oncolysis, Gene. Ther. 11 (2004) 214–223.
[22] J.T. Wu, H.M. Byrne, D.H. Kirn, L.M. Wein, Modeling and analysis of a virus that replicates selectively in tumor cells, Bull. Math. Biol. 63 (2001) 731–768.
[23] J.T. Wu, D.H. Kirn, L.M. Wein, Analysis of a three-way race between tumor growth, a replication-competent virus and an immune response, Bull. Math. Biol. 66 (2004) 605–625.